The response of methane hydrate beneath the seabed offshore Svalbard to ocean warming during the next three centuries

Héctor Marín-Moreno,[1] Timothy A. Minshull,[1] Graham K. Westbrook,[1] Bablu Sinha,[2] and Sudipta Sarkar[1,3]

Received 6 September 2013; accepted 22 September 2013; published 3 October 2013.

[1] Methane is a potent greenhouse gas and large-scale rapid release of methane from hydrate may have contributed to past abrupt climate change inferred from the geological record. The discovery in 2008 of over 250 plumes of methane gas escaping from the seabed of the West Svalbard continental margin at ~400 m water depth (mwd) suggests that hydrate is dissociating in the present-day Arctic. Here we model the dynamic response of hydrate-bearing sediments over a period of 2300 years and investigate ocean warming as a possible cause for present-day and likely future dissociation of hydrate, within 350–800 mwd, west of Svalbard. Future temperatures are given by two climate models, HadGEM2 and CCSM4, and scenarios, Representative Concentration Pathways (RCPs) 8.5 and 2.6. Our results suggest that over the next three centuries 5.3–29 Gg yr^{-1} of methane may be released to the Arctic Ocean on the West Svalbard margin. **Citation:** Marín-Moreno, H., T. A. Minshull, G. K. Westbrook, B. Sinha, and S. Sarkar (2013), The response of methane hydrate beneath the seabed offshore Svalbard to ocean warming during the next three centuries, *Geophys. Res. Lett.*, *40*, 5159–5163, doi:10.1002/grl.50985.

1. Introduction

[2] Significant amounts of methane carbon are contained in hydrate-bearing sediments along continental margins, and 100–600 Gt may be stored in the Arctic [*Archer et al*., 2009]. Hydrate forms at low temperature-high pressure conditions and if the dissolved methane concentration in the sediments within the gas hydrate stability zone (GHSZ) is at saturation value. Hydrate is most sensitive to global warming at high latitudes and in shallow water depths [e.g., *Hunter et al*., 2013]. Previous modeling studies of hydrate dissociation at continental margins, using simple future climate-change scenarios, suggest that increasing temperature will liberate significant amounts of methane from hydrate to the oceans [e.g., *Nisbet*, 1989; *MacDonald*, 1990; *Reagan et al*., 2011], as may have happened during past warm periods [e.g., *Dickens*, 2011].

[3] West of Svalbard (Figure 1), modeling studies indicate that methane bubble plumes observed at 340–400 m water depth (mwd) [*Westbrook et al*., 2009] could originate from warming-induced hydrate dissociation [*Reagan et al*., 2011; *Thatcher et al*., 2013]. Rates of warming of 1–3°C per hundred years could yield gas at the seabed 70–100 years after the onset of warming [*Reagan et al*., 2011], but gas flow at the seabed could have been caused by a 1.0°C increase of the bottom water over the last three decades due to the increase in the temperature of the West Spitsbergen current in response to Atlantic warming. The timescale of response depends upon the effective permeability and upon the initial distribution of hydrate, which is itself dependent upon the history of hydrate formation and dissociation [*Thatcher et al*., 2013].

[4] Here we model the future dynamic behavior of hydrates west of Svalbard using temperature series over the next three centuries given by two climate models, HadGEM2 [*Collins et al*., 2011a, 2011b] and CCSM4 [*Gent et al*., 2011], and two future climate-forcing scenarios, Representative Concentration Pathways (RCPs) 8.5 and 2.6 [*Moss et al*., 2010], which represent high and low greenhouse emissions, respectively. The models employ the TOUGH+HYDRATE code [*Moridis et al*., 2012], with constraints on input parameters from seismic observations.

2. Modeling Approach

[5] We generated eight different 1-D models for water depths of 350, 400, 420, 450, 500, 600, 700, and 800 m. Each model was initialized with the seabed temperature at 1 CE, hydrostatic pressure, a constant heat flow in the entire column, hydrate-free sediment in the top 7 m to approximate the sulphate reduction zone, and saturations of hydrate within and gas below the GHSZ of 5% and 3–4% of pore space, respectively. We imposed a constant heat flow, instead of a constant geothermal gradient, because the gradient changes with the phase (hydrate, water, or gas) occupying the pore space. Seabed temperature series for the period 1–2300 years (Figures 2a, 2b, and supporting information, Figure S1) were constructed for each water depth modeled using mean annual seabed temperatures given by climate models HadGEM2 and CCSM4 under RCPs scenarios 8.5 and 2.6 for the period 2005–2300, except for that from CCSM4 model RCP 8.5 which ends at 2250, from oceanographic measurements for the period 1900–2005 and from foraminifera proxy data for the period 1–1900. For the time frame of our analysis, changes in global sea level [e.g., *Grinsted et al*., 2010] and isostatic rebound [*Forman et al*., 2004] affecting the gas hydrate system are likely to be minor compared to ocean warming, and so they are not considered here.

[6] Our initial hydrate saturation of 5% of the pore space lies between the 6–13%, estimated for the same area from

Additional supporting information may be found in the online version of this article.

[1]National Oceanography Centre, Southampton, University of Southampton, Southampton, UK.
[2]National Oceanography Centre, Southampton, UK.
[3]Now at GEOMAR, Helmholtz Centre for Ocean Research, Kiel, Germany.

Corresponding author: H. Marín-Moreno, National Oceanography Centre, Southampton, University of Southampton, Waterfront Campus, European Way, Southampton, SO14 3ZH, UK. (hector.moreno@noc.soton.ac.uk)

0094-8276/13/10.1002/grl.50985

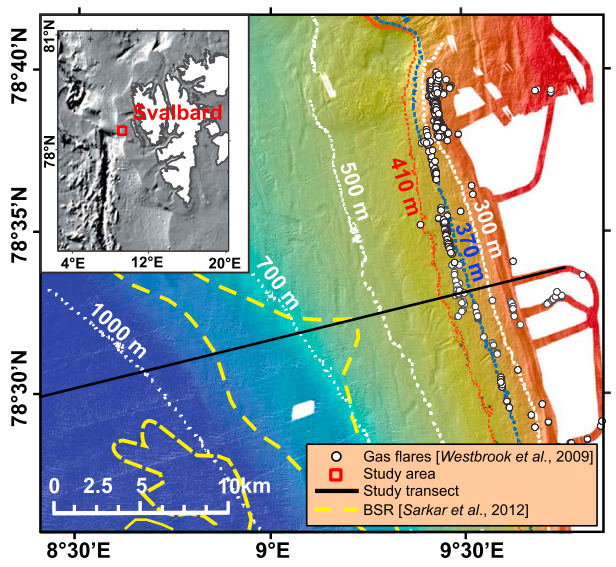

Figure 1. Map of the study area with bathymetry derived from multibeam echo-sounding data acquired on Cruise JR211. The dotted blue and red bathymetric contours represent the upper limit of the modeled steady state bottom of the gas hydrate stability zone (GHSZ) at 2°C and 3°C seabed water temperatures, respectively, and assuming a 3.5 wt% salinity, pure methane hydrate, and hydrostatic pressures [*Sarkar et al.*, 2012].

P and *S* wave velocities in water depths of ~1285–1500 m and less than 5%, estimated in water depths of 480–866 m [*Chabert et al.*, 2011]. Initial gas saturation below the GHSZ of 3–4% of pore space is consistent with values of 1–7% calculated for the same area within water depths of 480–1285 m [*Chabert et al.*, 2011]. We assumed a gas composition of 100% methane in our models, consistent with gas samples collected at the seabed from bubble plumes in the water column, showing a hydrocarbon composition of 99.9% methane (less than 0.01% ethane) [*James et al.*, 2011]. During the production runs, we introduced a source of basal heat flow that is constant over time, but varies with water depth, equal to the heat flow used as an initial condition. The imposed heat flows are such that the calculated depths of the base of the GHSZ for the initial models at 600, 700, and 800 mwd, assuming a constant thermal conductivity for water saturated sediments of 1.4 W $m^{-1}K^{-1}$, are similar to the depths of the bottom-simulating reflector (BSR) at those water depths, interpreted from nearby seismic reflection data [*Sarkar et al.*, 2012]. At water depths shallower than 600 m, the BSR cannot be identified, and we set the heat flow at 500–350 mwd equal to that at 600 mwd. Also, based on seismic velocities [*Chabert et al.*, 2011; *Sarkar et al.*, 2012], we limited the thickness of the zone containing hydrate to be less than ~100 m, and used a simplified two-layer model of glaciogenic sediments on top of marine sediments for water depths shallower than

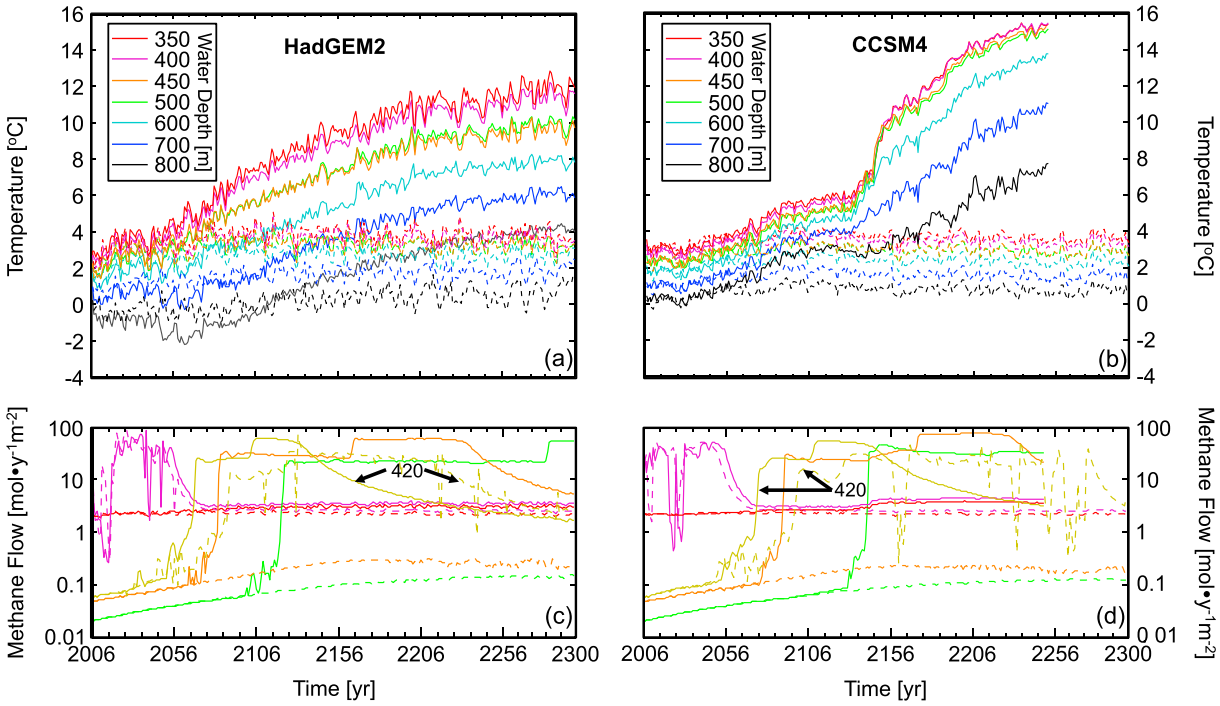

Figure 2. Results using temperatures from climate models (a and c) HadGEM2 and (b and d) CCSM4 at our study transect (Figure 1) for the period 2006–2300 years. Solid lines show results using the climate-forcing scenario RCP 8.5 and dashed lines using RCP 2.6. (Figures 2a and 2b) Future temperature for 800, 700, 600, 500, 450, 400, and 350 meters water depth (mwd). (Figures 2c and 2d) Methane flow at the seabed for 350 (red lines), 400 (purple lines), 420 (yellow-green lines), 450 (brown lines), and 500 (green lines) mwd. Note that the first jump in methane outflow observed at 420, 450, and 500 mwd for both climate models and RCP 8.5 is due to dissociation from the top part of the gas hydrate layer, and the second jump occurs when methane from dissociated hydrate at the base of the GHSZ reaches the seabed and contributes to the methane outflow.

600 m, and a one-layer model comprising just marine sediments in deeper water. We imposed a porosity of 0.3 for the glaciogenic sediments, to account for their very poor sorting [*Thatcher et al*., 2013], and of 0.5 for the marine sediments. Using *Budiansky's* [1970] method, a sediment porosity of 0.5 corresponds to a thermal conductivity for water-saturated sediments of 1.4 W $m^{-1}K^{-1}$. Recently measured values in the top few meters of sediment in the plume area are 1.8–2.1 W $m^{-1}K^{-1}$ (T. Feseker, personal communication, 2011), but such high values lead to overestimation of the depth of the base of the GHSZ, interpreted from seismic data to be about 20 m below seafloor (mbsf) at 400 mwd. Therefore, we used a thermal conductivity of 1.4 W $m^{-1}K^{-1}$ for both sediment types.

[7] We tested intrinsic permeabilities of 10^{-16}–10^{-12} m^2, and for values greater than 10^{-14} m^2, the rate of free methane gas transport from dissociated hydrate to the seabed was similar and limited by the rate at which the latent heat required to dissociate the hydrate could be supplied. The extent to which fracture permeability enhances the effective permeability in this setting is not clear, but in models with a low permeability (10^{-16} m^2) the pore pressure exceeded the lithostatic load only a few years after the dissociation of hydrate commenced and the effective permeability required for the system to respond in the time frame of the most recent period of warming of the seabed (about 30 years) is ~10^{-13} m^2 [*Thatcher et al*., 2013]. Therefore, following them, we used an intrinsic permeability of 10^{-13} m^2, which is two orders of magnitude higher than that used by other authors [*Reagan et al*., 2011]. We also accounted for changes in intrinsic permeability and capillary pressure arising from changes in the degrees of hydrate and ice saturation in the pore space. The irreducible gas saturation was 2%, consistent with other modeling studies in water-gas-hydrate systems and with laboratory measurements [*Reagan et al*., 2011; *Thatcher et al*., 2013]. We imposed a constant methane flow at the bottom of the model that approximately matched the rate of flow of gas already in the column. We included multiphase molecular diffusion and, hence, methane could be transported by gas flow, by advection of dissolved methane in the aqueous phase, and by molecular diffusion of methane in the aqueous and gas phases. Methane flux by molecular diffusion is slow compared with the other two mechanisms, but for the long time periods considered here it becomes important. A summary of the physical properties of the gas hydrate system and seismic constraints is shown in the supporting information (Table S3).

3. Results and Discussion

[8] There are several aspects of modeling of the response of methane-hydrate system west of Svalbard to increasing ocean temperature presented here that have not been undertaken in previous published modeling studies. The predictions of future changes in climate come from published global climate models. The initial model was chosen so that, when "grown" over the past 2000 years and driven by a model of changing ocean temperature, it provided a present-day subseabed distribution of gas and hydrate that is close to that indicated by seismic data, that image the BSR in water depths of more than 580 m and the upper limit of gas-related reflectors in shallower water. Therefore, our predictions regarding the future behavior of the gas hydrate system and on methane emissions from dissociated hydrate are driven by present-day observations rather than assumptions about initial conditions (supporting information, Model Uncertainties).

[9] The resulting initial conditions produce no hydrate 2000 years ago at 350 mwd. At 400 mwd, methane hydrate would have started to dissociate at about 850 CE, and dissolved methane would have been transported to the seabed by advection at a rate of about 0.1–0.3 mol yr^{-1} m^{-2} until ~1930 CE (supporting information, Figure S1b). Then, due to the increase in temperature over the Industrial Period, gas hydrates would have destabilized at 400 mwd and, ~15 years later, free methane gas would have started to be released to the Arctic Ocean with a maximum methane flow of 100 mol yr^{-1} m^{-2} (supporting information, Figure S1). However, very few of the acoustically imaged bubble plumes reach the sea surface [*Westbrook et al*., 2009]. Even if the bubbles could reach the seabed with significant size, for water depths deeper than 100 m, most of the original methane may be dissolved into the water column and replaced by other gases [*McGinnis et al*., 2006], increasing ocean acidification. Once there is a constant amount of free gas above the irreducible gas saturation within the GHSZ, the pulses of seabed methane are directly correlated with changes in temperature with no time delay (see insets in supporting information, Figure S1). By ~2050 CE, most hydrate dissociates (Figure 3 and supporting information, Figure S3), but it takes ~30 years more for all of the liberated methane to migrate to the ocean (Figures 2c and 2d).

[10] At 400 mwd the future response of the system is not sensitive to which climate model and RCP scenario is used. At the present day, most of the system is out of the GHSZ, with the base of the gas hydrate at ~20 mbsf (Figure 3 and supporting information, Figure S3). The uncertainty in its future response to ocean warming is small. Between 420 and 500 mwd, the response of the gas hydrate system depends on the climate model and RCP scenario considered (Figures 2c, 2d, 3 and supporting information, Figure S3). At 420 mwd, with the HadGEM2 model, methane gas reaches the seabed at ~2090 CE and at ~2068 CE if using RCP 2.6 or RCP 8.5, respectively. With the CCSM4 model, methane reaches the seabed at ~2097 CE and at ~2075 CE if using RCP 2.6 or RCP 8.5, respectively. At 450 mwd, hydrate at the base of the GHSZ starts to dissociate at ~2065 CE with the HadGEM2 model and at ~2075 CE with the CCSM4 model, for both climate scenarios. However, no free methane gas arrives at the seabed in either model when using climate scenario RCP 2.6 and hence, the methane from dissociated hydrate just increases the saturation of gas hydrate at shallower depths (Figure 3 and supporting information, Figure S3). At this water depth and using RCP 8.5, methane gas starts to be released to the ocean at ~2085 CE with the HadGEM2 model and at ~2095 CE with the CCSM4 model, with a maximum methane flow of 70 mol yr^{-1} m^{-2} (Figures 2c and 2d). At 500 mwd, whereas with climate scenario RCP 2.6 the system is stable and no dissociation occurs in either climate model, with RCP 8.5 free methane gas from dissociated hydrate would start to be released to the water column at ~2100 CE with the HadGEM2 model and at ~2130 CE with the CCSM4 model, with a maximum seabed methane flow of 55 mol yr^{-1} m^{-2} (Figures 2c and 2d).

[11] The timing differences between the models at 400–500 mwd result from lower temperatures estimated by the CCSM4 model over the next century. At water depths deeper than

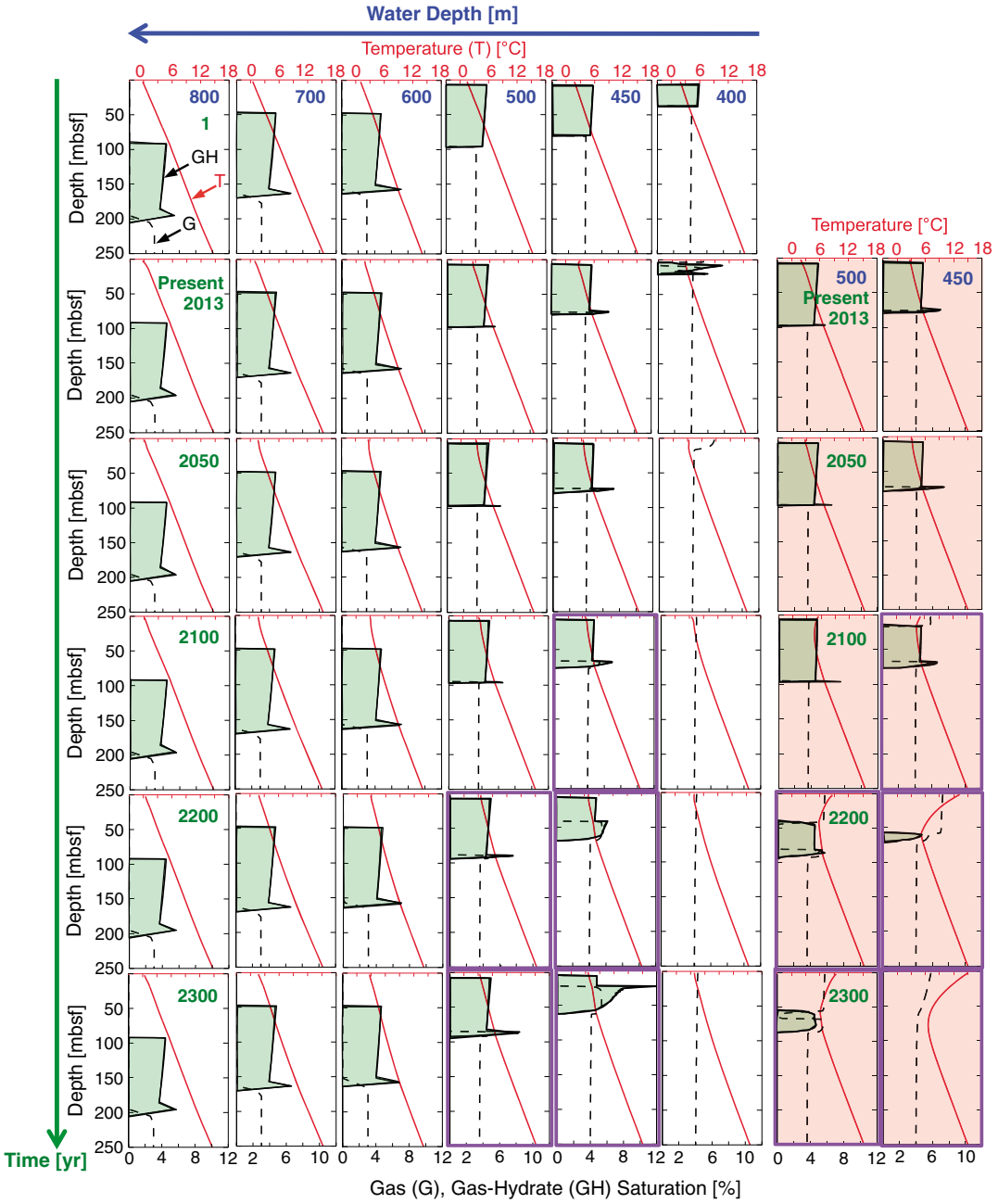

Figure 3. (left) Grid of results showing the variations in temperature (T, solid red lines), and saturations of gas hydrate (GH, solid black lines enclosing green areas) and gas (G, dashed black lines) with time (rows) and water depth (columns), using the climate model HadGEM2 and climate-forcing scenario RCP 2.6. Each individual plot in the grid shows the variation of T, and of GH and G saturations with depth for a specific water depth and time. (right) Plots with red backgrounds show the results using the climate model HadGEM2 and RCP 8.5. The plots outlined in purple show that, at 2100–2300 years and at 450–500 mwd, the differences between the results from using RCP 2.6 and RCP 8.5 are significant.

~500–600 m, hydrate remains stable for the time period considered (Figure 3 and supporting information, Figure S3). At water depths where there are methane emissions, the period of high rate emissions increases with increasing water depth (Figures 2c and 2d), because the amount of hydrate beneath the seabed in the models increases with increasing water depth and the magnitude of high rate emissions is similar at different water depths and limited by enthalpy [*Thatcher et al.*, 2013].

[12] We estimated the methane flow in the area where gas hydrate dissociation occurs, between latitudes of 78° 26′N–78°40′N (~25 km length), assuming a constant continental slope of 1.5°, between the 370 and 500 mwd contours in Figure 1, to calculate the across-margin distance. The time averaged methane flows at 400, 420, 450, 500, and 600 mwd over a time period and per square meter of area, were calculated from the total methane liberated over that period at each water depth, and the time averaged methane flows between the water depths modeled were estimated from a linear interpolation. Over the next century, the gas hydrate dissociation front may retreat an across-margin distance of 2860

m from ~400 to ~480 mwd (Figure 2c). Therefore, within this depth range, the methane release per meter wide strip across margin will be 0.11–0.33 Mg yr^{-1} and for the 25 km long dissociation area will be 3.9–6.6 Gg yr^{-1} (2.4–7.2 mol yr^{-1} m^{-2}) if using RCP 2.6 or RCP 8.5, respectively. Over the next three centuries, the active gas hydrate dissociation area may occupy 134 km^2 (seabed range of ~400–550 mwd) releasing 5.3–29 Gg yr^{-1} (2.5–13.5 mol yr^{-1} m^{-2}) if using RCP 2.6 or RCP 8.5, respectively. Although the flux per square meter is limited by enthalpy, the total flux over the next three centuries increases with time because the active area of methane emission increases.

[13] If our calculations for the next three centuries can be extended to an area of seabed within 400–550 mwd of ~41400 km^2 along the Svalbard archipelago (73°N–85°N; 0–40.4°E), and to an area of ~152,350 km^2 along the entire Eurasian Margin [*Jakobsson et al*., 2008], the potential methane release from marine hydrate over the next three centuries may be ~1.7–9 Tg yr^{-1} and ~6.1–33 Tg yr^{-1}, respectively. Such extrapolations should be treated with caution because current ocean temperatures (colder further east, so involving hydrate in shallower waters), slopes (more gentle in shallow waters, so dissociation perhaps affecting a larger area), and future temperature changes will vary along the margin. However, even considering the entire Eurasian Margin, the maximum potential methane release from hydrate is about five times smaller than global methane emissions from all natural wetlands, which are currently ~150 Tg yr^{-1} [*Dlugokencky et al*., 2011], the same order of magnitude as the 8–29 Tg yr^{-1} from Arctic tundra [*McGuire et al*., 2012], and about two orders of magnitude smaller than the 5000 Tg yr^{-1} from the East Siberian Arctic Shelf recently assumed by *Whiteman et al*. [2013].

[14] **Acknowledgments.** This work was supported by the UK Department of Energy and Climate Change through a supplement to Natural Environment Research Council grants NE/H002732/1 and NE/H022260/1. We thank Matt Hornbach and an anonymous reviewer for their detailed and constructive comments.

[15] The Editor thanks two anonymous reviewers for their assistance in evaluating this paper.

References

Archer, D., B. Buffett, and V. Brovkin (2009), Ocean methane hydrates as a slow tipping point in the global carbon cycle, *Proc. Natl. Acad. Sci. U. S. A.*, *106*(49), 20,596–20,601, doi:10.1073/pnas.0800885105.

Budiansky, B. (1970), Thermal and thermoelastic properties of isotropic composites, *J. Compos. Mater.*, *4*(3), 286–295, doi:10.1177/002199837000400301.

Chabert, A., T. A. Minshull, G. K. Westbrook, C. Berndt, K. E. Thatcher, and S. Sarkar (2011), Characterization of a stratigraphically constrained gas hydrate system along the western continental margin of Svalbard from ocean bottom seismometer data, *J. Geophys. Res.*, *116*, B12102, doi:10.1029/2011JB008211.

Collins, W. J., et al. (2011a), Development and evaluation of an Earth-System model – HadGEM2, *Geosci. Model Dev.*, *4*, 1051–1075, doi:10.5194/gmd-4-1051-2011.

Collins, W. J., et al. (2011b), The HadGEM2-ES implementation of CMIP5 centennial simulations, *Geosci. Model Dev.*, *4*, 543–570, doi:10.5194/gmd-4-543-2011.

Dickens, G. R. (2011), Down the Rabbit Hole: Toward appropriate discussion of methane release from gas hydrate systems during the Paleocene-Eocene thermal maximum and other past hyperthermal events, *Climate Past*, *7*(3), 831–846, doi:10.5194/cp-7-831-2011.

Dlugokencky, E. J., E. G. Nisbet, R. Fisher, and D. Lowry (2011), Global atmospheric methane: Budget, changes and dangers, *Philos. Trans. R. Society A*, *369*(1943), 2058–2072, doi:10.1098/rsta.2010.0341.

Forman, S., D. Lubinski, Ó. Ingólfsson, J. Zeeberg, J. Snyder, M. Siegert, and G. Matishov (2004), A review of postglacial emergence on Svalbard, Franz Josef Land and Novaya Zemlya, northern Eurasia, *Quat. Sci. Rev.*, *23*(11), 1391–1434, doi:10.1016/j.quascirev.2003.12.007.

Gent, P. R., G. Danabasoglu, L. J. Donner, M. M. Holland, E. C. Hunke, S. R. Jayne, D. M. Lawrence, R. B. Neale, P. J. Rasch, and M. Vertenstein (2011), The community climate system model version 4, *J. Clim.*, *24*(19), 4973–4991, doi:10.1175/2011JCLI4083.1.

Grinsted, A., J. C. Moore, and S. Jevrejeva (2010), Reconstructing sea level from paleo and projected temperatures 200 to 2100 AD, *Clim. Dyn.*, *34*(4), 461–472, doi:10.1007/s00382-008-0507-2.

Hunter, S. J., D. S. Goldobin, A. M. Haywood, A. Ridgwell, and J. G. Rees (2013), Sensitivity of the global submarine hydrate inventory to scenarios of future climate change, *Earth Planet. Sci. Lett.*, *367*, 105–115, doi:10.1016/j.bbr.2011.03.031.

James, R. H., D. P. Connelly, C. Graves, B. Alker, C. Cole, I. Wright, and A. Kolomijeca (2011), Fate of methane released from Arctic shelf and slope sediments and implications for climate change. AGU Fall Meeting, 2011.

Jakobsson, M., R. Macnab, L. Mayer, R. Anderson, M. Edwards, J. Hatzky, H. W. Schenke, and P. Johnson (2008), An improved bathymetric portrayal of the Arctic Ocean: Implications for ocean modeling and geological, geophysical and oceanographic analyses, *Geophys. Res. Lett.*, *35*, L07602, doi:10.1029/2008gl033520.

MacDonald, G. J. (1990), Role of methane clathrates in past and future climates, *Clim. Change*, *16*(3), 247–281, doi:10.1007/BF00144504.

McGinnis, D., J. Greinert, Y. Artemov, S. Beaubien, and A. Wüest (2006), Fate of rising methane bubbles in stratified waters: How much methane reaches the atmosphere?, *J. Geophys. Res.*, *111*, C09007, doi:10.1029/2005JC003183.

McGuire, A. D., et al. (2012), An assessment of the carbon balance of Arctic tundra: Comparisons among observations, process models, and atmospheric inversions, *Biogeosciences*, *9*(8), 3185–3204, doi:10.5194/bg-9-3185-2012.

Moridis, G. J., M. B. Kowalsky, and K. Pruess (2012), TOUGH+HYDRATE v1.2 user's manual: A code for the simulation of system behavior in hydrate-bearing geological media, Per. LBNL-0149E, Lawrence Berkeley Natl. Lab., Berkeley, Calif.

Moss, R. H., J. A. Edmonds, K. A. Hibbard, M. R. Manning, S. K. Rose, D. P. van Vuuren, T. R. Carter, S. Emori, M. Kainuma, and T. Kram (2010), The next generation of scenarios for climate change research and assessment, *Nature*, *463*(7282), 747–756, doi:10.1038/nature08823.

Nisbet, E. (1989), Some northern sources of atmospheric methane: Production, history, and future implications, *Can. J. Earth Sci.*, *26*(8), 1603–1611, doi:10.1139/e89-136.

Reagan, M. T., G. J. Moridis, S. M. Elliott, and M. Maltrud (2011), Contribution of oceanic gas hydrate dissociation to the formation of Arctic Ocean methane plumes, *J. Geophys. Res.*, *116*, C09014, doi:10.1029/2011JC007189.

Sarkar, S., C. Berndt, T. A. Minshull, G. K. Westbrook, D. Klaeschen, D. G. Masson, A. Chabert, and K. E. Thatcher (2012), Seismic evidence for shallow gas-escape features associated with a retreating gas hydrate zone offshore west Svalbard, *J. Geophys. Res.*, *117*, B09102, doi:10.1029/2011JB009126.

Thatcher, K. E., G. K. Westbrook, S. Sarkar, and T. A. Minshull (2013), Methane release from warming-induced hydrate dissociation in the West Svalbard continental margin: Timing, rates, and geological controls, *J. Geophys. Res. Solid Earth*, *118*, 22–38, doi:10.1029/2012JB009605.

Westbrook, G. K., et al. (2009), Escape of methane gas from the seabed along the West Spitsbergen continental margin, *Geophys. Res. Lett.*, *36*, L15608, doi:10.1029/2009GL039191.

Whiteman, G., C. Hope, and P. Wadhams (2013), Climate science: Vast costs of Arctic change, *Nature*, *499*, 401–403, doi:10.1038/499401a.